energies

MDPI

Article

Assessment of Metal Foil Pump Configurations for EU-DEMO

Xueli Luo *, Yannick Kathage, Tim Teichmann, Stefan Hanke, Thomas Giegerich and Christian Day

Institute for Technical Physics, Karlsruhe Institute of Technology, Hermann-von-Helmholtz-Platz 1, 76344 Eggenstein-Leopoldshafen, Germany; yannick.kathage@kit.edu (Y.K.); tim.teichmann@kit.edu (T.T.); stefan.hanke@kit.edu (S.H.); thomas.giegerich@kit.edu (T.G.)

* Correspondence: xueli.luo@kit.edu

Abstract: It is a challenging but key task to reduce the tritium inventory in EU-DEMO to levels that are acceptable for a nuclear regulator. As solution to this issue, a smart fuel cycle architecture is proposed based on the concept of Direct Internal Recycling (DIR), in which the Metal Foil Pump (MFP) will play an important role to separate the unburnt hydrogen isotopes coming from the divertor by exploiting the superpermeation phenomenon. In this study, we will present the assessment of the performance of the lower port of EU-DEMO after the integration of the MFP. For the first time, a thorough comparison of three different MFP (parallel long tubes, sandwich and halo) designs is performed regarding conductance for helium molecules, the pumping speed and the separation factor for deuterium molecules under different physical and geometric parameters. All simulations were carried out in supercomputer Marconi-Fusion with our in-house Test Particle Monte Carlo (TPMC) simulation code ProVac3D because the code had been parallelized with high efficiency. These results are essential for the development of a suitable MFP design in the vacuum-pumping train of EU-DEMO.

Keywords: Direct Internal Recycling (DIR); Test Particle Monte Carlo (TPMC) simulation; Metal Foil Pump (MFP); pumping speed; separation factor

Citation: Luo, X.; Kathage, Y.; Teichmann, T.; Hanke, S.; Giegerich, T.; Day, C. Assessment of Metal Foil Pump Configurations for EU-DEMO. *Energies* **2024**, *17*, 3889. https://doi.org/10.3390/en17163889

Academic Editor: Guglielmo Lomonaco

Received: 18 June 2024
Revised: 31 July 2024
Accepted: 5 August 2024
Published: 7 August 2024

1. Introduction

Nuclear fusion is a promising long-term option for a sustainable, non-carbon-emitting global energy supply, and Tokamak is a fusion reactor where the deuterium–tritium nuclear fusion takes place in a well-controlled plasma confinement.

EU-DEMO is a next-generation Tokamak in plan within the framework of the EUROfusion Consortium. It is foreseen to operate in pulsed mode: the plasma will be heated to achieve nuclear fusion in the burn phase. In the dwell phase, the magnetic field coils of the Tokamak are recharged and the vessel is evacuated down to a base pressure in the mPa regime for pulse preparation [1]. One challenging but key task in EU-DEMO is to reduce the tritium inventory to levels that are acceptable for a nuclear regulator [2]. As a solution to this issue, a smart fuel cycle architecture is proposed based on the concept of Direct Internal Recycling (DIR), as shown in Figure 1 [3]. Here, a Metal Foil Pump (MFP) separates a large fraction of the unburnt hydrogen isotopes coming from the divertor [4–6] by exploiting a phenomenon called superpermeation. This introduces a short-cut in the fuel cycle for the unburnt fuel and greatly reduces the size of the separation stages in the tritium plant, thus reducing the tritium inventory.

The MFP is foreseen to be installed inside the DEMO lower port as shown in Figure 2 and the downstream primary pumping is planned as linear diffusion pumps with a baffle system at the inlet [7–10]. The lower port is of complex geometry, contains various pipe routings, and will be used as the port for remote maintenance activities. In the burn phase of the Tokamak, the lower port must provide not only the necessary pumping speed for helium and Plasma Enhancement Gases (PEGs), but also the necessary pumping speed and sufficient separation efficiency for hydrogen isotopes in the torus exhaust gas mixture. The

MFP does not have to be operated in the dwell phase since there is no significant throughput of fuel to be separated. Therefore, it will only impose an additional vacuum conductance resistance during dwell, which has to be considered during system design. Obviously, it is a hard task in the MFP design to meet all these requirements in both operational phases of EU-DEMO, and three different MFP design configurations are proposed.

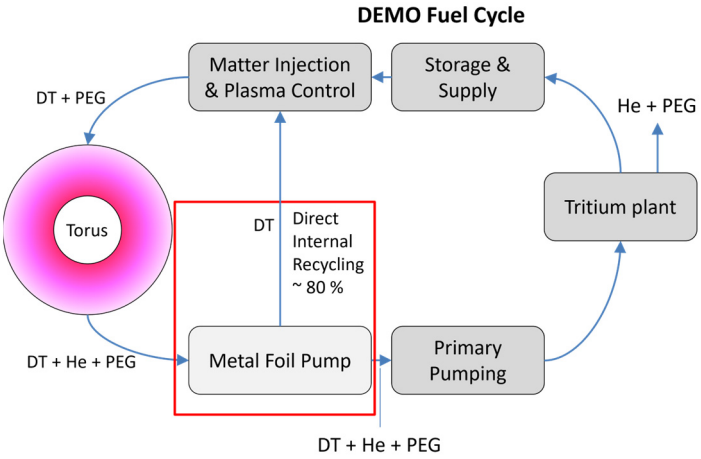

Figure 1. Smart fuel cycle architecture of EU-DEMO.

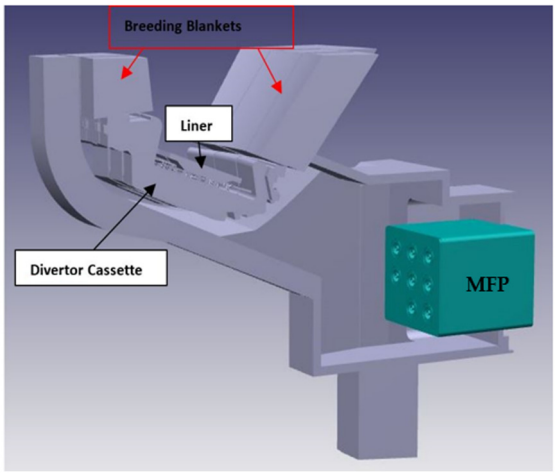

Figure 2. The lower port after the integration of the MFP.

In this paper, a thorough assessment of the system performance by means of the Test Particle Monte Carlo (TPMC) simulations will be presented. Generally, the TPMC method is only suitable for free-molecular flow. In this case, molecules can be simulated individually because the interactions between the gas molecules are negligible. Considering a free-molecular flow in steady state, the residence time of individual molecules on the wall of the system and in the system is not relevant, and the conductance and the pumping speed of the system can be derived from the simulation results of the trajectories of a huge number of test particles [11].

In the dwell phase, the flow in the divertor-pumping path of EU-DEMO is in a free-molecular flow regime and in transition regime during burn, as the pressure close to the divertor is in the order of 1 Pa then. Thus, the free-molecular flow assumption leads to conservative estimates for the pumping speeds and overestimates the amount of surface interactions of a particle before removal through the outlet of the MFP, leading to optimistic separation efficiencies. Nonetheless, since the flow regime is not far from free molecular, we assume that the results obtained from the simulation can already give valuable insights into the achievable performance range of the divertor-pumping path of EU-DEMO with different MFP designs. This approach with reasonable computational efforts is appropriate

in the current design stage. Once the plasma scenario for EU-DEMO is decided and the operational pressure range in the pump duct is known to cause transition flow, the most promising designs can be further quantified using a Direct Simulation Monte Carlo (DSMC) approach.

2. MFP Working Principle and Simulation Model

By definition, superpermeation implies that the permeation flow through a metal foil is at least 10% of incoming particles [12]. To characterize and quantify this effect, the experimental facility HERMESplus was set up at the Institute for Technical Physics of Karlsruhe Institute of Technology in Karlsruhe, Germany, and plasma-driven superpermeation was demonstrated through a thin niobium foil (0.1 mm thick) at about hundred times higher fluxes than regular gas-driven permeation [4,5].

This process is illustrated in Figure 3. In the upstream (left) side, hydrogen is dissociated in the gas phase to produce hydrogen atoms, which possess the energy to absorb into the metal at high probabilities despite the presence of a non-metallic impurity surface layer [13]. This layer suppresses molecular dissociation on the surface of the metal, thus greatly reducing the absorption caused by impingement of hydrogen molecules. Hydrogen with the ability to absorb at high probabilities despite the surface energy barrier is also referred to as suprathermal hydrogen. Once absorbed, hydrogen can diffuse to the downstream side of the foil, giving rise to large permeation fluxes. The key to superpermeation is the suppression of the upstream recombination of absorbed hydrogen caused by the surface impurity layer. On the downstream side of the foil, hydrogen is routed through the DIR loop by primary pumps. As the driving force of superpermeation is the concentration gradient of suprathermal hydrogen, which should not be present on the downstream side of the foil, this process (i) can pump against a pressure gradient and (ii) is selective for energetic hydrogen.

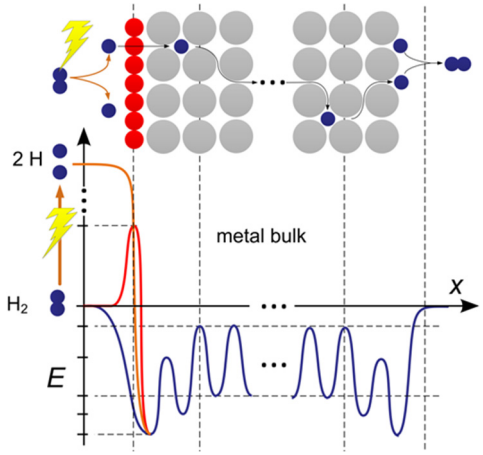

Figure 3. Scheme of the hydrogen superpermeation process.

Our in-house Test Particle Monte Carlo code ProVac3D, which has been validated and widely used in different nuclear fusion applications [14,15], is upgraded to distinguish the hydrogen molecules in normal and suprathermal states, which are denoted as mQ and eQ (number of the molecule without unit in this study), respectively. In order to simulate their evolution processes and permeation inside an MFP, as illustrated by the schematic in Figure 4, several phenomenological parameters are introduced based on our experimental data.

On the boundary of the plasma source:

- When hydrogen molecules enter the MFP inlet as mQ, they can be excited to eQ at the temperature of the plasma source and the excitation probability is c2e; the residual of mQ (1 − c2e) will reflect as mQ without temperature change.

- eQ will reflect on the plasma boundary at the temperature of the plasma source. However, eQ can recombine into mQ at a recombination probability of c2er = 0.02 [16].

On the metal foil:

- The permeation probability of eQ is c1e, and the residual of eQ (1 − c1e) will reflect at the temperature of the metal foil, in which eQ is possible to recombine into mQ and the recombination probability is taken as c1r = c1e.
- All ground-state particles mQ are reflected as such and take on the temperature of the metal foil upon collision with it.

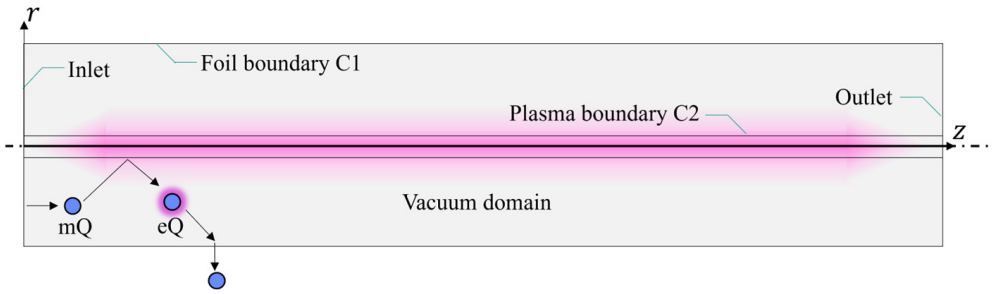

Figure 4. Exemplary schematic illustrating the basic idea behind the simulation model.

Under the assumption of the molecular flow in this study, a hydrogen molecule will be defined as mQ after it has left the MFP either from the inlet or from the outlet because it will hit the wall of the divertor-pumping path in the simulation domain. Of course, these parameters have no effect on the helium gas molecules and the MFP functions only as a conductive duct for the helium gas flow in the whole divertor-pumping path. Since the purpose of this study is to help the selection of the right configuration of MFPs by systematic simulations of the system performance of different configurations of MFPs, all evolution probabilities are assumed as constants independent of the temperature under the first-order approximation.

Three different designs of the MFP, as shown in Figure 5, are studied in this paper. The dimensions of the MFP in all three designs are L = 2.27 m, width W = 2.4 m and height H = 2.1 m. In the sandwich design (Figure 5a), there are two channels of the width b = 0.75 m and height h = 2.1 m, with two arrays of four plasma sources of d = 0.05 m diameter each, and with vertical foil segments as the sides of the channels. In the tube design (Figure 5b), there are eight cylindrical tubes with an outer diameter D = 0.5 m, at which cylindrical metal foils are installed. The plasma source is installed in the center of the cylinder. In the halo design (Figure 5c), there are two concentric tubes made of metal foils, and the diameters of the inner tube and the outer tube are D_1 = 0.6 m and D_2 = 1.8 m, respectively; eight plasma sources of d = 0.05 m are circularly distributed between the inner and outer tubes. In addition, a horizontal tube of a diameter of 0.2 m close to the MFP outlet in the sandwich design is foreseen and the mechanical structures to support the plasma sources in three designs, such as the bars or rings close to the MFP inlet and outlet, are also simplified and included in the simulation model. Thus, the most important cross-sections in the MFP are the torus exhaust flow cross-section as well as the permeate flow cross-section as part of the DIR loop.

It is noted that we did not study the stand-alone MFP, but assessed the system performance of the lower port of EU-DEMO after the MFP is installed (Figure 2). The two interfaces of the whole simulation model are as follows: (1) The system inlet is chosen as the interface to the divertor. After considering that a small part is blocked by the breeding blanket, it is simulated by 42 triangles with a total area A = 5.62 m^2. (2) The system outlet is chosen as the flange to connect with the baffle system of the downstream linear diffusion pumps [9,10], and a small volume between the MFP and the flange is also included in the simulation model. The width and height of the system outlet is 1.6 m and 1.9 m, respectively.

So, the area of it is A′ = 3.04 m^2. The sticking coefficient of this system outlet is denoted as stk.

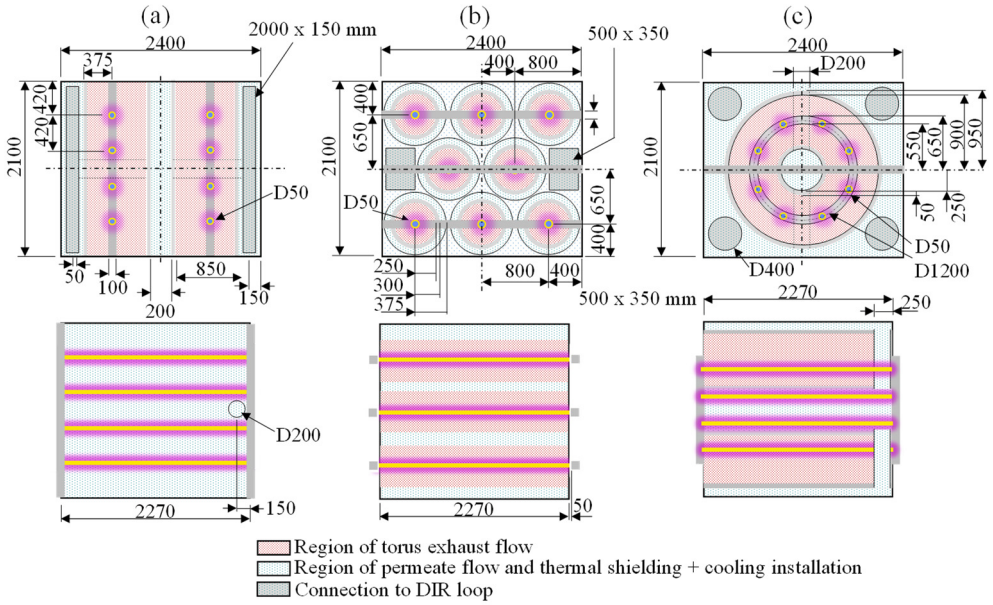

Figure 5. Sandwich design (**a**), 8-tube design (**b**) and halo design (**c**), and their main geometrical dimensions.

The temperature of the metal foil is 873 K; the temperature of the plasma source is 1000 K; the temperature of the supporting structure for the plasma sources is 570 K; the other components of the system are at a temperature of 20 °C. The reflection from a normal component except the metal foil and the plasma source is considered as the diffuse reflection with total thermal accommodation. To accelerate the simulation, the MFP inlet and outlet (different to the system inlet and outlet) are considered as the virtual control surfaces, and, in this way, we can also check the correctness of the simulation from the flow conservations of the test molecules. All simulations were carried out using the EUROfusion high-performance computer Marconi-Fusion at the Cineca, Italy. Because our code ProVac3D is successfully parallelized with very good speed-up efficiency [17], this very complicated system was systematically simulated by 10^{11} to 10^{12} test molecules with 200 to 2000 CPUs.

3. Helium Transmission Probability

To simulate the helium transmission probability of the whole system, test helium molecules at 570 K come from the system inlet (the interface to the divertor) and the sticking coefficient of the system outlet (the flange) is taken as a black hole of stk = 1. If n test helium gas molecules can exit the system outlet, the transmission probability is $w = n/n\_mc$, and n_mc is the total number of the test molecules in simulation (10^{11} or 10^{12}). The corresponding system conductance for the helium molecules is estimated by

$$C = \frac{1}{4}\langle v \rangle \mathrm{A} w, \tag{1}$$

where A = 5.62 m^2 is the area of the system inlet, and <v> = 1245 m/s is the thermal speed of helium @ 20 °C (ambient temperature).

It is easy to see from Table 1 that the helium transmission probability of the whole system is small and dominated by the MFP (bottleneck of the helium gas flow). Moreover, this value is almost proportional to the total opening area of the MFP, and for the helium, the order of the conductance of the whole system with the MPF is sandwich > halo > 8-tube.

Table 1. System performance of three different designs for helium.

Design	Total MF Area (m^2)	Total MFP Inlet Area (m^2)	w	Conductance (m^3/s)
Sandwich	19.07	3.15	0.104	182.25
8-tube	28.53	1.56	0.040	70.26
Halo	17.12	2.26	0.081	140.89

4. Deuterium Pumping Speed and Separation Factor

The simulations are performed with D_2 coming from the divertor at 570 K, and they may permeate the pump walls made of metal foils according to the designs shown in Figure 5. The sticking coefficient of the system outlet is estimated as stk = 0.04 to mimic the effective pumping speed of the downstream linear diffusion pumps with a special baffle system [9,10]. From the simulated pumping probability by the permeation on the metal foils w_{per} and the pumping probability by the system outlet (the flange) w_{flange}, we know the system total pumping probability is $w_{total} = w_{per} + w_{flange}$, and the system pumping speed S and the separation factor P are derived from

$$S = \frac{1}{4}\langle v \rangle \mathrm{A} w_{total}, \tag{2}$$

and

$$P = \frac{w_{per}}{w_{total}}, \tag{3}$$

where A = 5.62 m^2 is the system inlet area (the interface to the divertor), and <v> = 1731.1 m/s as the thermal speed of input deuterium molecules at 570 K. P is the ratio of the D_2 gas amount bypassed by the MFP because w_{per} denotes the pumping probability by the plasma-aided superpermeation on the metal foil walls of the MFP and w_{total} denotes the total pumping probability of the system.

In order to evaluate the effect of the permeation probability c1e and the excitation probability c2e, their values are chosen as c1e = 0.05, 0.1, 0.15, and 0.2, and c2e = 0.03, 0.045, 0.055, 0.125, 0.15, 0.175, 0.25, 0.35, and 0.45. In addition, the effective permeation probability of eQ (as well as the effective recombination probability) depending on the axial position of the test molecule inside the MFP is introduced as follows:

$$\mathrm{c1e}_z = \left(-0.0236z^3 + 0.0085z^2 - 0.0755z + 1.0226\right)c1e. \tag{4}$$

This function is experimentally determined according to the relative change in permeation with noble gas enrichment along the MFP axis, and z (from 0 to 2.27 m) denotes the distance from the MFP inlet. Because the factor on c1e in Equation (4) is smaller than unity, $\mathrm{c1e}_z$ is smaller than c1e, which is confirmed in all simulations.

Tables 2 and 3 list the simulation results of the system pumping speed S and the separation factor P. It is easy to know that S and P will increase with the permeation probability c1e and the excitation probability c2e, and all three designs will deliver the highest system pumping speed and highest separation factor under the best combination of permeation and excitation (c1e = 0.2 and c2e = 0.45).

In order to compare the performance of these different designs, Figures 6 and 7 show individual dependencies of S and P on c1e and c2e, respectively. In general, the order of the system pumping speed is sandwich > halo > 8-tube; the order of the system separation efficiency is 8-tube > halo > sandwich. Since these two orders are opposing, the design with the lowest pumping speed achieves the highest separation factor for deuterium gas molecules, which means a trade-off should be made in the selection of the MFP design.

Table 2. System pumping speed S of three different designs for D_2.

	8-Tube Design				Sandwich Design				Halo Design			
S(m^3/s)	**c1e = 0.05**	**c1e = 0.1**	**c1e = 0.15**	**c1e = 0.2**	**c1e = 0.05**	**c1e = 0.1**	**c1e = 0.15**	**c1e = 0.2**	**c1e = 0.05**	**c1e = 0.1**	**c1e = 0.15**	**c1e = 0.2**
c2e = 0.03	41.04	42.87	43.79	44.34	48.73	50.96	52.46	53.54	47.05	49.29	50.68	51.63
c2e = 0.045	43.80	46.46	47.79	48.59	50.51	53.81	56.02	57.61	49.09	52.38	54.42	55.80
c2e = 0.055	45.56	48.75	50.34	51.30	51.68	55.67	58.35	60.27	50.41	54.38	56.84	58.51
c2e = 0.125	56.56	62.92	66.06	67.96	59.43	67.96	73.62	77.65	58.96	67.27	72.35	75.79
c2e = 0.15	59.99	67.31	70.90	73.08	62.03	72.05	78.67	83.38	61.75	71.45	77.35	81.34
c2e = 0.175	63.20	71.39	75.41	77.84	64.54	75.99	83.53	88.88	64.42	75.42	82.10	86.61
c2e = 0.25	71.70	82.16	87.25	90.32	71.64	87.03	97.08	104.16	71.75	86.28	95.03	100.90
c2e = 0.35	80.96	93.79	100.01	103.75	80.16	100.13	113.03	122.06	80.22	98.68	109.71	117.07
c2e = 0.45	88.50	103.19	110.29	114.56	87.76	111.68	126.99	137.64	87.48	109.20	122.10	130.66

Table 3. System separation factor of three different designs for D_2.

	8-Tube Design				Sandwich Design				Halo Design			
P	**c1e = 0.05**	**c1e = 0.1**	**c1e = 0.15**	**c1e = 0.2**	**c1e = 0.05**	**c1e = 0.1**	**c1e = 0.15**	**c1e = 0.2**	**c1e = 0.05**	**c1e = 0.1**	**c1e = 0.15**	**c1e = 0.2**
c2e = 0.03	0.178	0.223	0.244	0.257	0.084	0.129	0.158	0.177	0.104	0.151	0.179	0.196
c2e = 0.045	0.245	0.301	0.327	0.342	0.121	0.182	0.219	0.244	0.147	0.210	0.245	0.268
c2e = 0.055	0.283	0.345	0.373	0.389	0.143	0.213	0.255	0.282	0.173	0.245	0.284	0.308
c2e = 0.125	0.467	0.544	0.576	0.595	0.270	0.376	0.433	0.469	0.315	0.418	0.469	0.500
c2e = 0.15	0.511	0.589	0.621	0.639	0.306	0.419	0.477	0.513	0.352	0.461	0.513	0.544
c2e = 0.175	0.547	0.625	0.657	0.675	0.337	0.455	0.515	0.551	0.385	0.497	0.550	0.581
c2e = 0.25	0.628	0.704	0.734	0.750	0.414	0.539	0.598	0.634	0.463	0.579	0.631	0.661
c2e = 0.35	0.696	0.768	0.796	0.810	0.489	0.614	0.672	0.704	0.536	0.650	0.700	0.728
c2e = 0.45	0.741	0.809	0.834	0.848	0.543	0.666	0.720	0.751	0.586	0.698	0.746	0.772

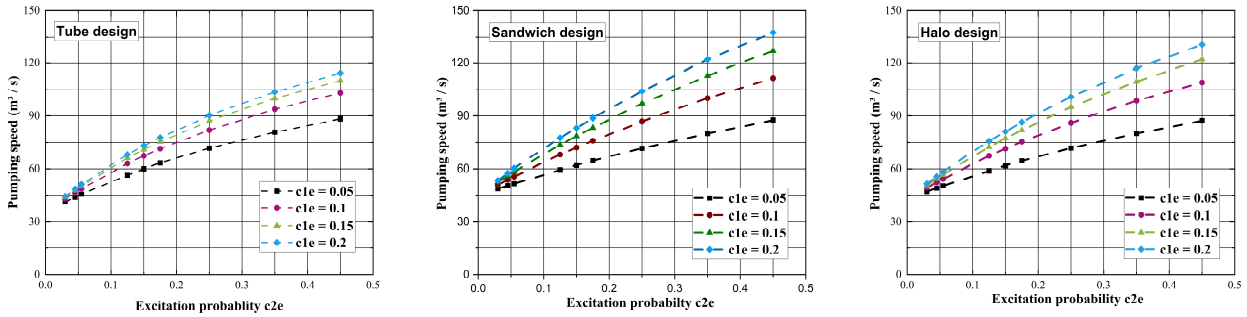

Figure 6. Pumping speed of 8-tube design (**left**), sandwich design (**middle**) and halo design (**right**).

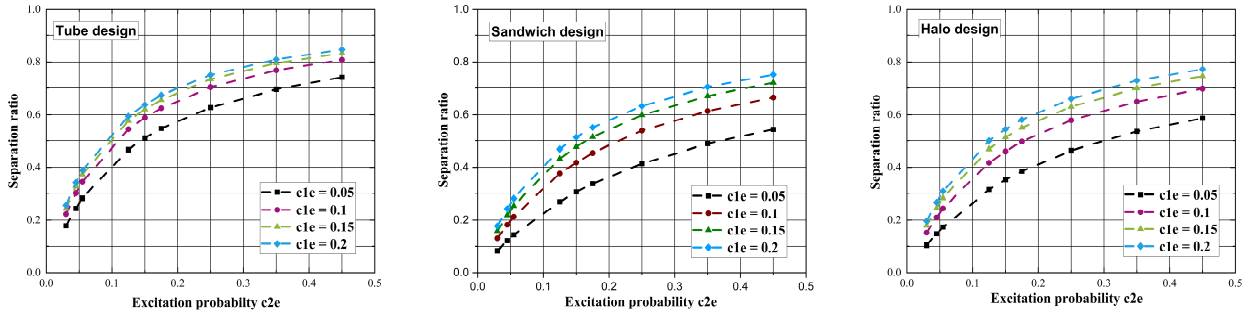

Figure 7. Separation factor of 8-tube design (**left**), sandwich design (**middle**) and halo design (**right**).

Please note that the required plasma power is the same for the three designs to allow for a better comparison, since all designs are equipped with eight plasma sources in total here. Considering also the manufacture and installation feasibility, together with the conductance for helium given in Section 3, the sandwich design is recommended as the most favorable design to meet the pumping requirements of EU-DEMO in the burn and dwell of a Tokamak.

5. Sensitivity Study of Geometrical and Physical Parameters in the Sandwich Design

5.1. Channel Width

In a study of the impact of channel width modification, moderate values of c1e = 0.1 and c2e = 0.35 are used, and the sticking coefficient on the system outlet (the flange) remains as stk = 0.04, supposing the same downstream pumping ability. Figure 8 shows that the He conductance increases with the width of the MFP channel but the separation ratio for D_2 decreases. However, the pumping speed for D_2 approximately remains the same for the investigated parameter space.

5.2. Sticking Coefficient (stk) of the System Outlet

To evaluate the impact of the outlet sticking coefficient, a channel width of 0.85 m is chosen for the sandwich design with two channels. Simulations were carried out with D_2; the permeation probability is c1e = 0.1 and the plasma excitation probability is c2e = 0.1, 0.35, and 0.45. The sticking coefficient on the system outlet is adjustable by closing the valve connecting to the primary pumps downstream. Figure 9b shows that as stk decreases, the separation ratio P increases since more deuterium gas molecules are reflected from the system outlet and have more chances to permeate through the metal foils. Obviously, when the valve on top of the linear diffusion pump is totally closed (stk = 0), $w_{flange} = 0$ and the separation factor will be in unity (Equation (3)). However, as shown in Figure 9a, the total pumping speed will decrease as stk decreases because D_2 molecules are also more likely to be forced to flow back to the divertor. And, as expected, the overall performance (both S and P) will increase as c2e increases.

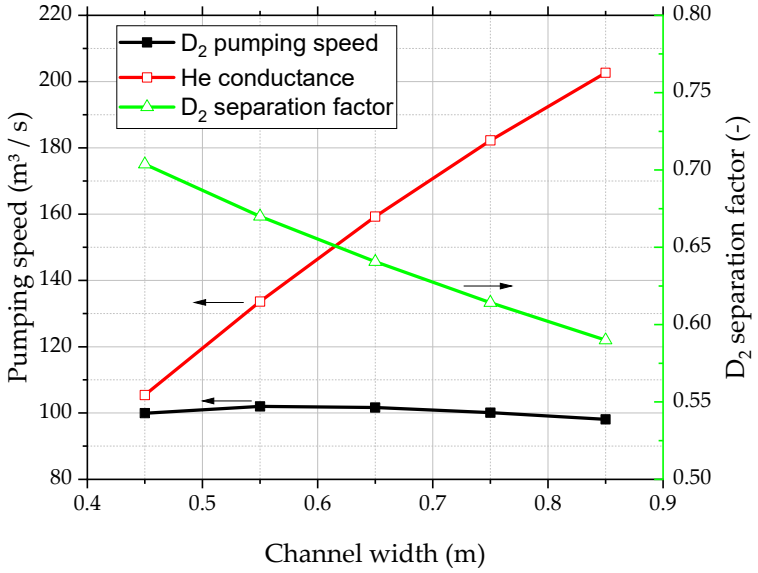

Figure 8. System performance versus the channel width in sandwich design.

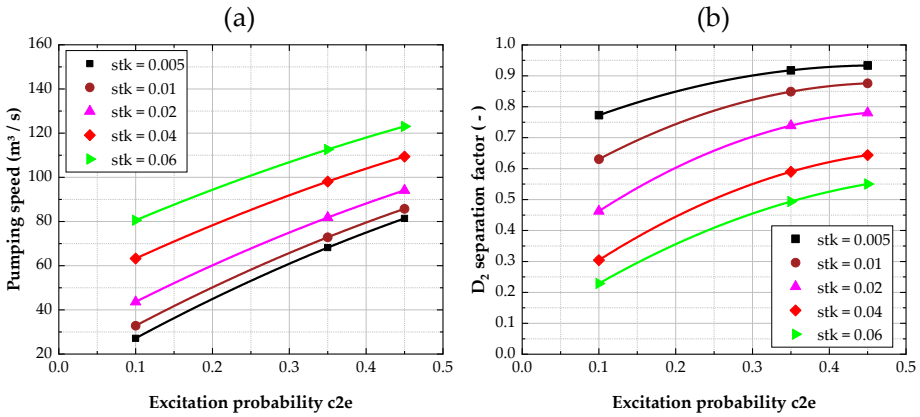

Figure 9. System performance versus the sticking coefficient of the system outlet. (**a**) Pumping speed; (**b**) D_2 separation factor.

5.3. Number of Plasma Sources in One Channel

In another study, the effect of introducing more plasma sources is analyzed. For this, the channel width is chosen as 0.85 m for the sandwich design with two channels. Moderate values of c1e = 0.1 and c2e = 0.35 for D_2 are used, and the sticking coefficient on the system outlet remains as stk = 0.04, supposing the same downstream pumping ability. As shown in Table 4, both S and P for D_2 gas will increase as the number of plasma sources in one MFP channel (M) increases. Of course, the total number of plasma sources is 2 × M, and more M means more required power to supply the plasma sources.

Table 4. D_2 pumping speed and separation factor versus the number of plasma sources (M) in one channel.

M	Pumping Speed S (m^3/s)	Separation Ratio P
4	98.09	0.5900
5	107.37	0.6353
6	116.91	0.6746
7	124.62	0.7019
8	132.43	0.7264

5.4. Configuration with Three Channels

It would be possible to have three channels for the sandwich design in the same space, with a channel width of 0.52 m and wall thickness of 0.21 m. The total metal foil area in this design is 28.602 m^2 and the system conductance for helium is simulated as 165.56 m^3/s, which is slightly lower than the value in the two-channel design when the channel width is 0.75 m.

In D_2 simulation, moderate values of c1e = 0.1 and c2e = 0.35 are used, and the sticking coefficient on the system outlet remains as stk = 0.04, supposing the same downstream pumping ability. Figure 10 shows that the system performance (both S and P for D_2) improves (better than the corresponding values in the two-channel design when the channel width is 0.85 m) at the cost of 1.5 times more total plasma sources in the three-channel design than in the two-channel design.

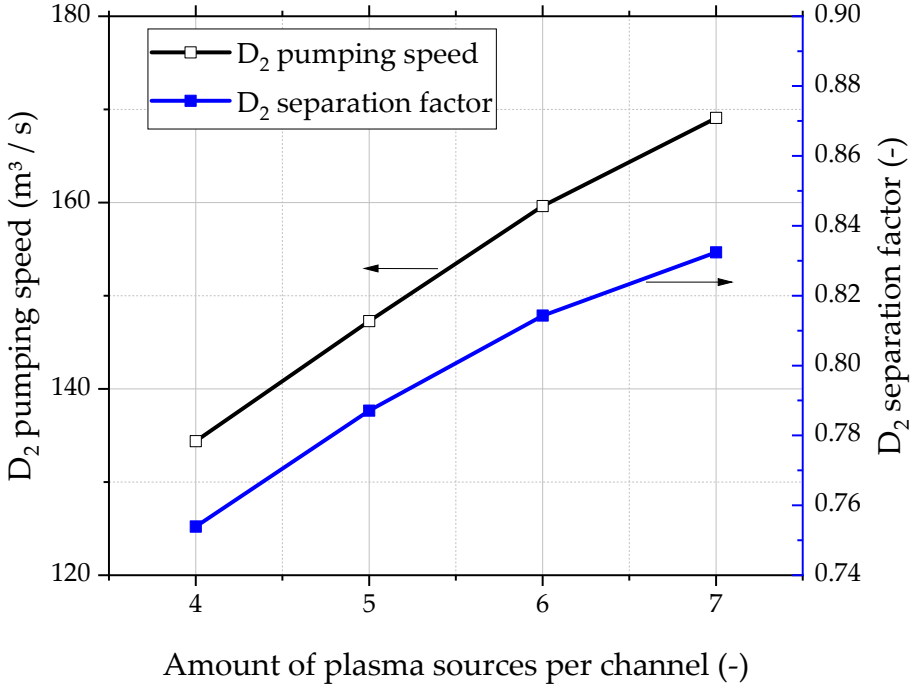

Figure 10. S and P of D_2 of the sandwich design with 3 channels.

6. Conclusions

The DEMO divertor-pumping path of very complex geometry and the system performance with the MFPs were successfully simulated with the Test Particle Monte Carlo simulation code ProVac3D. Because the code was parallelized with high efficiency, we can systematically simulate the whole integral pumping path from the divertor interface to the flange connecting the baffle system of the downstream primary pumping system in supercomputer Marconi-Fusion. The assessments of three different MFP configurations (parallel long tubes, sandwich and halo) are presented and the values of the transmission probability of helium and PEGs, and the pumping speed and the separation factor of the hydrogen isotopes when both the permeation probability and the excitation probability vary in a big range, are obtained. It is found that the divertor-pumping path integrated with the MFP of the sandwich configuration would have the highest helium conductance of 182 m^3/s and the highest deuterium pumping speed of 137 m^3/s. As for the hydrogen isotope separation, the divertor-pumping path with the MFP in sandwich configuration would deliver a moderate separation efficiency of 75%, and it can be improved by changing its geometrical and physical parameters. These results are important for us to choose a suitable and feasible MFP design and physical and geometrical parameters to meet pumping requirements in both burn and dwell phases of a Tokamak. In addition, the results are useful for identification of the necessary number of pumping ports and for further system

development and optimization to define simulation boundary conditions for the upstream system and the downstream system, i.e., the divertor and the diffusion pump, respectively.

Author Contributions: Conceptualization, X.L., Y.K., T.T., S.H., T.G. and C.D.; Methodology, X.L., Y.K. and T.T.; Software, X.L.; Validation, X.L., Y.K., S.H. and T.G.; Formal analysis, X.L.; Investigation, Y.K., T.T. and S.H.; Writing—original draft, X.L. and Y.K.; Writing—review & editing, X.L., Y.K. and T.T.; Visualization, X.L.,Y.K. and T.T.; Project administration, T.G. and C.D. All authors have read and agreed to the published version of the manuscript.

Funding: This work has been carried out within the framework of the EUROfusion Consortium, funded by the European Union via the Euratom Research and Training Programme (Grant Agreement No. 101052200—EUROfusion). Views and opinions expressed are, however, those of the author(s) only and do not necessarily reflect those of the European Union or the European Commission. Neither the European Union nor the European Commission can be held responsible for them.

Data Availability Statement: The original contributions presented in the study are included in the article, further inquiries can be directed to the corresponding author.

Acknowledgments: The simulations have been performed on the EUROfusion high-performance computer Marconi-Fusion. The authors gratefully acknowledge the resources granted to the project VAC_ND. Moreover, we acknowledge support by the KITPublication Fund of the Karlsruhe Institute of Technology.

Conflicts of Interest: The authors declare no conflict of interest.

References

1. Biel, W.; Backers, M.; Kemp, R.; Wenninger, R.; Zohm, H. Systems code studies on the optimization of design parameters for a pulsed DEMO tokamak reactor. *Fusion Eng. Des.* **2017**, *123*, 206–211. [CrossRef]
2. Federici, G.; Bachmann, C.; Barucca, L.; Biel, W.; Boccaccini, L.; Brown, R.; Bustreo, C.; Ciattaglia, S.; Cismondi, F.; Coleman, M.; et al. DEMO design activity in Europe: Progress and updates. *Fusion Eng. Des.* **2018**, *136*, 729–741. [CrossRef]
3. Day, C.; Giegerich, T. The Direct Internal Recycling concept to simplify the fuel cycle of a fusion power plant. *Fusion Eng. Des.* **2013**, *88*, 616–670. [CrossRef]
4. Peters, B.J.; Hanke, S.; Day, C. Metal Foil Pump performance aspects in view of the implementation of Direct Internal Recycling for future fusion fuel cycles. *Fusion Eng. Des.* **2018**, *136*, 1467–1471. [CrossRef]
5. Hanke, S.; Day, C.; Giegerich, T.; Igitkhanov, J.; Kathage, Y.; Luo, X.; Varoutis, S.; Cortes, A.V.; Härtl, T.; Busniuk, A.; et al. Progress of the R&D programme to develop a metal foil pump for DEMO. *Fusion Eng. Des.* **2020**, *161*, 111890.
6. Li, C.; Fuerst, T.F.; Way, J.D.; Wolden, C. Low temperature hydrogen superpermeation in vanadium composite metal foil pumps. *Nuclear Mater. Energy* **2023**, *37*, 101529. [CrossRef]
7. Giegerich, T.; Day, C.; Gliss, C.; Luo, X.; Strobel, H.; Wilde, A.; Jimenez, S. Preliminary configuration of the torus vacuum pumping system installed in the DEMO lower port. *Fusion Eng. Des.* **2019**, *146*, 2180–2183. [CrossRef]
8. You, J.H.; Mazzone, G.; Visca, E.; Greuner, H.; Fursdon, M.; Addab, Y.; Bachmann, C.; Barrett, T.; Bonavolontà, U.; Böswirth, B.; et al. Divertor of the European DEMO: Engineering and technologies for power exhaust. *Fusion Eng. Des.* **2022**, *175*, 113010. [CrossRef]
9. Day, C.; Battes, K.; Butler, B.; Davies, S.; Farina, L.; Frattolillo, A.; George, R.; Giegerich, T.; Hanke, S.; Härtl, T.; et al. The pre-concept design of the DEMO tritium, matter injection and vacuum systems. *Fusion Eng. Des.* **2022**, *179*, 113129. [CrossRef]
10. Teichmann, T.; Luo, X.; Giegerich, T.; Day, C. Study of the effective torus exhaust high vacuum pumping system performance in the inner tritium plant loop of EU-DEMO. *Fusion Sci. Technol.* **2024**, *80*, 399–410. [CrossRef]
11. Jousten, K. (Ed.) Chapter 5. Analytical and Numerical Calculations of Rarefied Gas Flows. In *Handbook of Vacuum Technology*, 2nd ed.; Wiley-VCH: Weinheim, Germany, 2016; ISBN 978-3-527-41338-6.
12. Livshits, A.I.; Notkin, M.E.; Samartsev, A.A. Physico-chemical origin of superpermeability—Large-scale effects of surface chemistry on "hot" hydrogen permeation and absorption in metals. *J. Nuclear Mater.* **1990**, *170*, 79–94. [CrossRef]
13. Hatano, Y.; Watanabe, K.; Livshits, A.; Busnyuk, A.; Alimov, V.; Nakamura, Y.; Hashizume, K.-I. Effects of bulk impurity concentration on the reactivity of metal surface: Sticking of hydrogen molecules and atoms to polycrystalline Nb containing oxygen. *J. Chem. Phys.* **2007**, *127*, 204707. [CrossRef] [PubMed]
14. Luo, X.; Hauer, V.; Day, C. Monte Carlo calculation of the thermal radiation heat load of the ITER pre-production cryopump. *Fusion Eng. Des.* **2012**, *87*, 603–607. [CrossRef]
15. Luo, X.; Scannapiego, M.; Day, C.; Sakurai, S. Assessment of the JT-60SA divertor cryopump performance. *Fusion Eng. Des.* **2018**, *136*, 467–471. [CrossRef]

16. St-Onge, L.; Moisan, M. Hydrogen atom yield in RF and microwave hydrogen discharges. *Plasma Chem. Plasma Process.* **1994**, *14*, 87–116. [CrossRef]
17. Luo, X.; Day, C. Topological impact of a simple self-replication geometric structure with great application potential in vacuum pumping and photovoltaic industry. *J. Vac. Sci. Technol. B* **2021**, *39*, 054203. [CrossRef]